Chapter 7

Analysis of Nonlinear Composite Members Including Bond-Slip

Manal K. Zaki

Additional information is available at the end of the chapter

http://dx.doi.org/10.5772/51446

1. Introduction

Extensive research has been carried out in recent years on the use of FRP composites in strengthening of RC structures. Concrete elements strengthened with FRP undergo significant improvement of strength, ductility and resistance to electrochemical corrosion. Moreover, strengthening concrete member with FRP has the advantages of decreased installation costs and repairs, less stiffness and weight in comparison with steel. The increase in stiffness of the structural elements is undesirable in seismic prone areas. Structural members can be strengthened with FRP jackets provided along the whole length of the member or in regions of maximum straining actions. FRP strengthening can, also, be provided on one face of the structural member as in the case of stiffening the tension fibers of a beam.

For FRP retrofitting problem, the confinement model describing the behavior of rectangular concrete columns retrofitted with externally bonded FRP material and subjected to axial stress was presented by Chaallal et al. [1]. Other researchers investigated the effect of FRP in seismic strengthening of concrete columns, Tastani and Pantazopoulou [2] and Ozcan et al. [3]. They found that FRP retrofitting remarkably increased the strength and ductility of the strengthened members. Some researchers proposed simplified equations for FRP retrofit design of difficient rectangular columns, Ozcan et al. [4].

Other researchers studied reinforced concrete members externally bonded with FRP fabric using commercial software ANSYS, Kachlakev et al. [5], Li et al. [6]. Yan et al. [7] developed an analytical stress-strain model. Purushotham et al. [8] studied piles in berthing structures under uniaxial bending. Kaba and Mahin [9] presented the concept of fiber method in their refined modeling of RC columns for seismic analysis under uniaxial bending.

Some searches were conducted to the problem of biaxial bending. Bresler [10] and Bernardo [11] studied biaxial bending for unretrofitted short rectangular columns.

At early stage of the use of layered beams, full interaction (perfect bond) was assumed in the design. It was until the mid-fifties that Newmark and his co-authors [12] pointed the influence of partial interaction on the overall elastic behavior of steel-concrete composite beams. They derived the governing equations and solved the equilibrium equations expressed in terms of the axial force. Since then, several studies have been conducted to study the problem of bond-slip, Arizumi et al. [13], Daniel and Crisinel [14], Salari et al. [15]. Gara [16] and Ranzi [17] adopted the displacement based finite element formulation to include the vertical slip. Salari et al. [18] also Valipour and Bradford [19] adopted one-dimensional element force-based element to solve the relevant problem. Other researchers [20] and [21] adopted the mixed-procedure, displacement-based together with force-based, to solve the problem. Moreover, nonlinear geometric effects were introduced to the problem by Girhammar and Gopu [22], Girhammar and Pan [23], Čas et al. [24] and Pi et al. [25]. Krawczyk and the co-authors [26,27], Battini et al. [28] developed a corotational formulation for the nonlinear analysis of composite beams with interlayer slip. Nguyen et al. [29], Sousa et al. [30] implemented a finite element model to solve a composite beam column with interlayer slip.

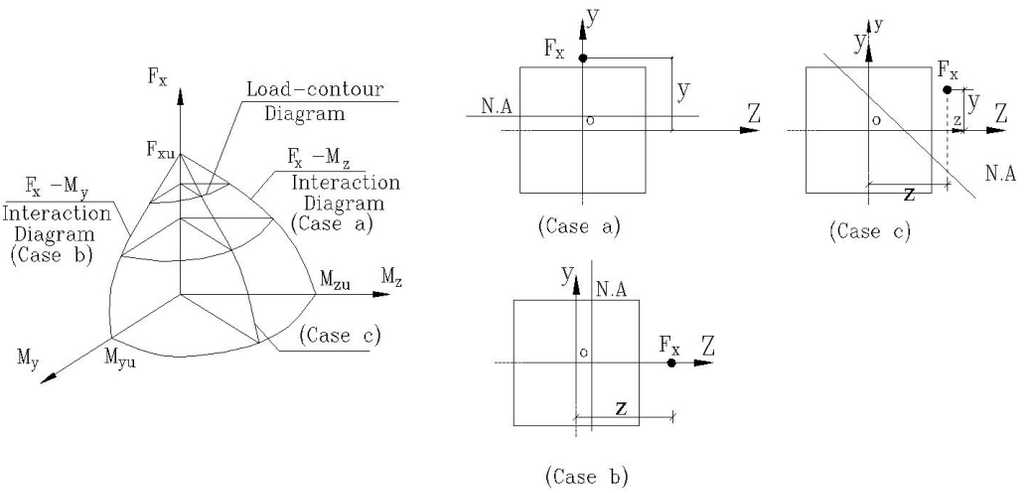

Figure 1. A typical interaction diagram of RC columns

In practice, many RC columns are subjected to biaxial bending. The analysis of such problems are difficult because a trial and adjustment procedure is necessary to find the inclination and depth of the neutral axis. The problem becomes more complicated when the slenderness effect is included. A typical interaction diagram for biaxially loaded column is shown in Fig. 1. Case a and case b are the uniaxial bending about the z axis and y axis respectively. The interaction curves represent the failure envelope for different combinations

http://dx.doi.org/10.5772/51446

of the axial load and bending moments. Case c represents the case of a RC column with biaxial bending.

The material nonlinearity is considered to account for concrete cracks and the change of the stress-strain relationship of the different materials. The material nonlinearity is thus introduced by using the FMM together with the incremental iterative solution. The geometric nonlinearity is considered in the present study to account for the deformations occurring due to excess bending moments developed by the effect of axial load. The geometric nonlinearity, thus, considers the slenderness effect of the column. The bond-slip effect is considered by introducing the bond properties of the epoxy resin applied to adhere FRP to the RC column.

The method adopted is accomplished by dividing the column into segments along the member axis to introduce the FEA for the skeletal segments. At each end of the segment, the cross-section is divided into concrete, steel and FRP fibers to introduce the FMM. The properties of a cross-section is calculated by summing up the properties of all the fibers or elemental areas of the particular section. The column segment properties are considered as the average properties of the its end cross-sections. The segment and cross-section discretization are detailed in section 2.

The load is applied incrementally until the maximum allowed strains are reached. An incremental iterative method is employed to solve the problem. After each iteration, the properties of each cross-section are computed according to the material changes occurring and governed by the stress-strain relationship for each material. The properties of each column segment is considered as the average between its end section properties. Those properties are then introduced to the tangential linear stiffness matrix. The geometric nonlinearity is accounted for through the geometric stiffness matrix. Also, the bond-slip effect is considered by the addition of the bond-slip stiffness matrix.

It is, therefore, the aim in this study to adopt the FEA to formulate the linear, geometric and the bond-slip stiffness matrices of composite members subjected to biaxial bending together with axial forces. The model is developed within an updated Lagrangian incremental formulation.

The assumptions of the present analysis are: 1)only longitudinal partial interaction is considered. Axial relative displacement occurs between different elements while the vertical displacement is the same for all elements. 2)small strains and moderate rotations are considered. This assumption represents a rigorous simplification applicable to many problems. 3) Both layers, referred to as elements in the present study, followed the Euler-Bernoulli beam theory. This considers that plane cross-sections remain plane after deformations and perpendicular to the axis of the beam. 4) Shear and torsional deformations are neglected. 5) Effect of the column weight is neglected.

2. Fiber method modelling of frp confined beam columns

The cross-section is divided into concrete, steel and FRP fibers to introduce The FMM is introduced herein to compute the properties of each fiber, thus achieving the properties of the

a cross-section by summing up the properties of all its fibers or elemental areas. The meshing is given in Fig. 2(a). The column segment properties are considered as the average properties of its end cross-sections.

The same derivation in the companion paper [31] for columns under biaxial bending is adopted herein after the necessary modifications to solve the column under the effect of slip.

The strain distribution is defined by the maximum compressive strain ε_m, together with the depth of the neutral axis, Z_n. The strains are shown in Fig. 2(b).

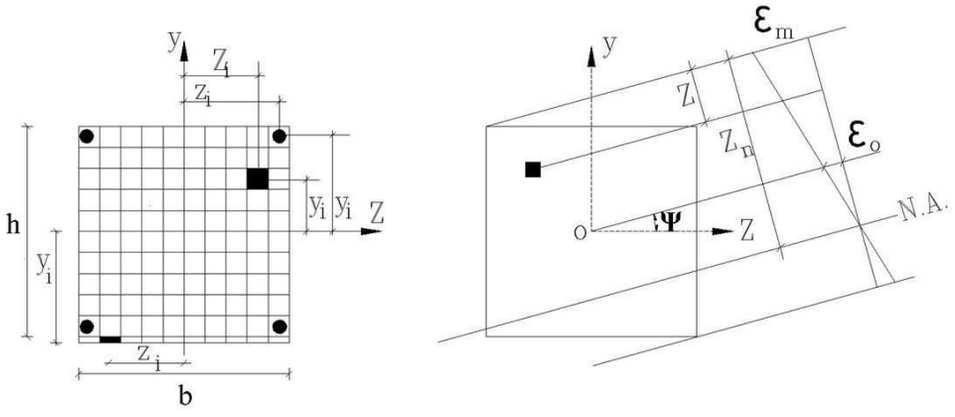

a. Discretization **b. Strains**

Figure 2. Cross-section

The following section parameters are then computed

$$\varepsilon_m = \varepsilon_o + \frac{b}{2}\phi_y + \frac{h}{2}\phi_z \tag{1}$$

$$\phi = \sqrt{\phi_y{}^2 + \phi_z{}^2} \tag{2}$$

$$z_n = \frac{\varepsilon_m}{\phi} \tag{3}$$

$$\Psi = \tan^{-1}\frac{\phi_z}{\phi_y} \tag{4}$$

where φ_y and φ_z are the curvatures along the y-axis and z-axis respectively and ε_o is the strain at point "O".

The elemental strain is computed as:

http://dx.doi.org/10.5772/51446

$$\varepsilon = \varepsilon_m(1 - \frac{Z}{Z_n}) \tag{5}$$

where Z is the distance from the maximum strain to the element measured perpendicular to the N.A. After determining the strain of each fiber from eq.5, the corresponding elemental modulus of elasticity, G, is determined as detailed in section 4. The elemental properties are computed and summed up to obtain the cross-section properties as shown in the following equations:

$$EA_\alpha = \sum_{i=1}^{nfib} [(G_i)\Delta A_i] \tag{6a}$$

$$EI_y = \sum_{\alpha=1}^{n} \left[\sum_{i=1}^{nfib} (z_i)^2 (G_i)\Delta A_i \right] \tag{6b}$$

$$EI_z = \sum_{\alpha=1}^{n} \left[\sum_{i=1}^{nfib} (y_i)^2 (G_i)\Delta A_i \right] \tag{6c}$$

$$EI_{yz} = \sum_{\alpha=1}^{n} \left[\sum_{i=1}^{nfib} (y_i)(z_i)(G_i)\Delta A_i \right] \tag{6d}$$

$$(ES_y)_\alpha = \sum_{i=1}^{nfib} [(z_i)(G_i)\Delta A_i] \tag{6e}$$

$$(ES_z)_\alpha = \sum_{i=1}^{nfib} [(y_i)(G_i)\Delta A_i] \tag{6f}$$

where α is the counter of an arbitrary element. In the present study, element 1 is the RC section and element 2 is the FRP. n is the total number of elements and is equal to 2 in the present study, i is the counter of fibers, $nfib$ is the total number of fibers of element α, ΔA_i is the area of each fiber, y_i, z_i are distances from the center of the considered fiber to the z and y axes respectively. Those symbols are shown in Fig. 2a. It should be noted that the properties EA, ES_y and ES_z are given separately for each element, while the properties EI_z, EI_y and EI_{yz} are the summation of the corresponding properties of both elements. The reason for this is that the axial displacement is different for each element due to the slip effect while both elements undergo the same curvatures about the z-axis and the y-axis.

3. Displacement-based fiber model with bond-slip

A one dimensional finite element analysis is adopted to solve the column segments. The segments are considered to be of unsymmetric cross-section caused by the inclination of the

N.A. The finite element formulation given by Yang and McGraw [32] to solve the thin-walled, i.e. bare-steel columns, is introduced herein after applying the necessary modification to include the concrete, FRP and bond-slip.

3.1. Displacements and strain fields

The axial displacement of an arbitrary point of an element (α) in the cross-section is given in terms of the displacements of a constant point "c" on the same element as follows

$$u_x = u_{xc\alpha} - zu'_{zc} - yu'_{yc} \tag{7}$$

where $u_{xc\alpha}$ is the axial displacement of the element α, y and z are the vertical and horizontal distances, respectively from the centroid of any follower element α to the centroid of the parent element having α=1. In the present study, the concrete section and the FRP are considered to be the parent and the follower elements respectively. And $u'_{yc} and u'_{zc}$ are the derivatives of the transverse displacements u_{yc} and u_{zc}.

$y=y_\alpha-y_1$ and $z=z_\alpha-z_1$ however, for simplicity, the reference axes are chosen such that $y_1=0$ and $z_1=0$, Fig.3 (a).

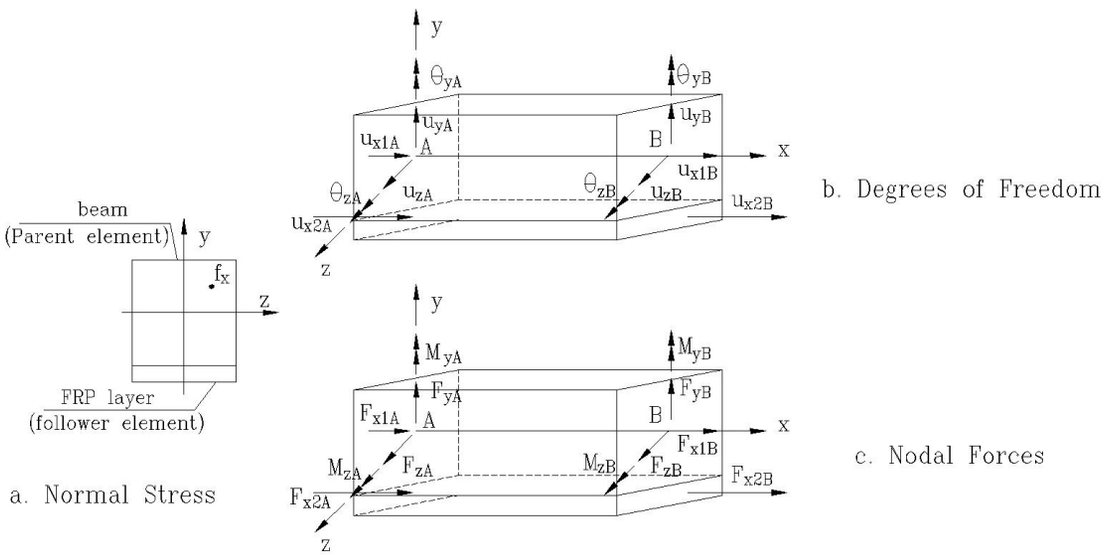

Figure 3. Column Segment

It should be noted that the transverse displacements, u_{yc} and u_{zc}, are considered to be the same for all elements of the beam with respect to the axis of the beam. For simplicity, the symbol "c" is dropped out from the r.h.s. of the equations. The relevant linear strain field can, then, be obtained from the displacement field given by eq. 7 by differentiating the mentioned equation w.r.t. the beam coordinates as

http://dx.doi.org/10.5772/51446

$$\varepsilon_{x\alpha} = (u_{x,x})_\alpha = u'_{x\alpha} - yu''_y - zu''_z \tag{8}$$

while the nonlinear strain field is given by

$$\eta_{xx} = \frac{1}{2}(u^2{}_{x,x} + u^2{}_{y,x} + u^2{}_{z,x}) \tag{9}$$

and $u_{x,x}$ is ignored as usual practice. The slip satisfying the compatibility relation with the displacements of element 1 and element 2 is given as

$$u_{xb} = u_{x2} - u_{x1} = u_{x2} - u_{x1} + zu_z^{'} + yu_y^{'} \tag{10}$$

3.2. Forces

In general, the the normal stress f_x shown in Fig. 3 (a) is expressed as

$$f_x = E_\alpha(u'_{x\alpha} - zu''_z - yu''_y) \tag{11}$$

Following the integrations at the cross-section, the stress resultant are expressed as

$$F_x = \int_A f_x dA \quad M_y = \int_A f_x z dA \quad M_z = -\int_A f_x y dA \tag{12}$$

$$F_x = EAu'_x - E(S_y)(u''_z) - E(S_z)(u''_y) \tag{13a}$$

$$M_y = -EI_y u''_z + E(S_y)(u'_x) - E(I_{yz})(u''_y) \tag{13b}$$

$$M_z = EI_z u''_y - E(S_z)(u'_x) + E(I_{yz})(u''_z) \tag{13c}$$

where the elemental properties are previously given in section 2.

3.3. Degrees of freedom and nodal forces

The local coordinates are shown in Fig. 3(b and c).

The displacement vector <u>is given by:

$$< u >=< u_{x1A} \quad u_{yA} \quad u_{zA} \quad \theta_{yA} \quad \theta_{zA} \quad u_{x2A} \quad u_{x1B} \quad u_{yB} \quad u_{zB} \quad \theta_{yB} \quad \theta_{zB} \quad u_{x2B} > \tag{14}$$

where θy and θz are the angles of rotation of the section about y and z axis respectively.

While the vector of the nodal forces <f> is given by:

$$< f >=< F_{x1A} \;\; F_{yA} \;\; F_{zA} \; M_{yA} \;\; M_{zA} \;\; F_{x2A} \;\; F_{x1B} \;\; F_{yB} \; F_{zB} \; M_{yB} \;\; M_{zB} \; F_{x2B} > \tag{15}$$

3.4. Virtual work

The partial interaction problem is solved using the principle of virtual work. This is accomplished by equating the work of internal stresses to the work of external stresses in an incremental form. The principle of virtual work will be adopted to deduce:

-the linear and nonlinear stiffness matrices of a beam element which consist of an assemblage of two different

elements connected by deformable interface.

-the bond-slip stiffness matrix.

The equilibrium condition for the entire beam-column is then expressed by assembling the vectors and matrices defined for each segment according to the principle of finite elements.

The details are given below.

3.4.1. For the beam with FRP

$$\int_v (E_1 e_{xx} \delta_1 e_{xx})^1 dV + \int_v (f_x \delta_1 \eta_{xx})^1 dV = {}^2_1 R - {}^1_1 R \tag{16}$$

in which ${}_1e_{xx}$ and ${}_1\eta_{xx}$ are the linear and non-linear incremental strain respectively, f_x denotes the stress at C_1, E is the modulus of elasticity of the cross-section and ${}^2\,{}_1R$ and ${}^1\,{}_1R$ are the external virtual work at C_2 and C_1 respectively but both being measured at C_1 and ${}^2\,{}_2R$ = the external virtual work expression

substituting equations 8 into eq.16, we get

$$\tfrac{1}{2}\int_v (E\delta(u^2{}_{x,x})dV + \tfrac{1}{2}\int (f_x \delta(u^2{}_{y,x} + u^2{}_{z,x})dV = {}^2R - {}^1R \tag{17}$$

A linear displacement field is adopted for the axial displacement, u_x, and a cubic displacement field for other displacements. The incremental displacements are expressed as:

$$u_x = \prec n_1 \succ \{\bar{u}_x\} u_y = \prec n_3 \succ \{\bar{u}_y\} u_z = \prec n_3 \succ \{\bar{u}_z\} \tag{18}$$

where

http://dx.doi.org/10.5772/51446

$$\prec n_1 \succ = \prec 1-i \qquad \text{i} \succ \tag{19a}$$

$$\prec n_3 \succ = \prec 1-3i^2+2i^3 \qquad i-2i^2+i^3 \qquad 3i^2-2i^3 \qquad i^3-i^2 \succ \tag{19b}$$

in which i is given by the value $\frac{x}{l}$.

The nodal degrees of freedom ie., the ends A and B of the column segment are given by:

$$\left\{\bar{u}_x\right\}_\alpha = \prec u_{xA\alpha} \qquad u_{xB\alpha} \succ \tag{20a}$$

$$\left\{\bar{u}_y\right\} = \prec u_{yA} \qquad l\theta_{zA} \qquad u_{yB} \qquad l\theta_{zB} \succ \tag{20b}$$

$$\left\{\bar{u}_z\right\} = \prec u_{zA} \qquad -l\theta_{yA} \qquad u_{zB} \qquad -l\theta_{yB} \succ \tag{20c}$$

where l is the length of the segment.

3.4.1.1. The linear part

The linear part taken from eq. 17 is

$$\prec \delta u \succ [K_e]\{u\} = \sum_{\alpha=1}^{n} \left[\tfrac{1}{2} \int_v (E\delta(u^2{}_{x,x})dV \right] \tag{21}$$

in which α is the counter of the considered elements and n is their total number.

$$\prec \delta u \succ [K_e]\{u\} = \sum_{\alpha=1}^{n} \left[\tfrac{1}{2} \int_v (E_\alpha \delta(u'_{x\alpha} - yu''_y - zu''_z)^2 dV \right] \tag{22}$$

applying the properties of the cross-section given in eqs 6, the previous expression becomes

$$\begin{aligned} \prec \delta u \succ [K_e]\{u\} = \sum_{\alpha=1}^{n} [& \tfrac{1}{2} \int_0^l E_\alpha A_\alpha \delta \left(u'_{x\alpha}\right)^2 dx + \int_0^l (-E_\alpha S_{z\alpha})\delta(u''_y u'_{x\alpha})^2 dx \\ & + \int_0^l (-E_\alpha S_{y\alpha})\delta(u''_z u'_{x\alpha})^2 dx \\ & + \tfrac{1}{2} \int_0^l E_\alpha I_{z\alpha} \delta \left(u''_y\right)^2 dx + \tfrac{1}{2} \int_0^l (E_\alpha I_{y\alpha})\delta(u''_z)^2 dx + \int_0^l (E_\alpha I_{yz\alpha})\delta(u''_y u''_z) dx] \end{aligned} \tag{23}$$

Substituting the interpolation functions in eq. 18, the following equation applies

$$\begin{aligned}
&\prec \delta u \succ [K_e]\{u\} = \prec \delta u_{x\alpha} \succ \left[\sum_{\alpha=1}^{n}\int_0^1 \frac{E_\alpha A_\alpha}{l}\{n_1'\}\prec n_1' \succ di\right]\{u_{x\alpha}\} + \prec \delta u_z \succ \left[\sum_{\alpha=1}^{n}\int_0^1 \frac{E_\alpha I_{y\alpha}}{l^3}\{n_3''\}\prec n_3'' \succ di\right]\{u_z\} \\
&+ \prec \delta u_y \succ \left[\sum_{\alpha=1}^{n}\int_0^l (\frac{-E_\alpha s_{z\alpha}}{l^2})\{n_3''\}\prec n_1' \succ di\right]\{u_{x\alpha}\} + \prec \delta u_{x\alpha} \succ \left[\sum_{\alpha=1}^{n}\int_0^l (\frac{-E_\alpha s_{z\alpha}}{l^2})\{n_1'\}\prec n_3'' \succ di\right]\{u_y\} \\
&+ \prec \delta u_z \succ \left[\sum_{\alpha=1}^{n}\int_0^l (\frac{-E_\alpha s_{y\alpha}}{l^2})\{n_3''\}\prec n_1' \succ di\right]\{u_{x\alpha}\} + \prec \delta u_{x\alpha} \succ \left[\sum_{\alpha=1}^{n}\int_0^l (\frac{-E_\alpha s_{y\alpha}}{l^2})\{n_1'\}\prec n_3'' \succ di\right]\{u_z\} \\
&+ \prec \delta u_z \succ \left[\sum_{\alpha=1}^{n}\int_0^l (\frac{E_\alpha I_{y\alpha}}{l^3})\{n_3''\}\prec n_3'' \succ di\right]\{u_z\} + \prec \delta u_y \succ \left[\sum_{\alpha=1}^{n}\int_0^l (\frac{E_\alpha I_{z\alpha}}{l^3})\{n_3''\}\prec n_3'' \succ di\right]\{u_y\} \\
&+ \prec \delta u_z \succ \left[\sum_{\alpha=1}^{n}\int_0^l (\frac{E_\alpha I_{yz\alpha}}{l^3})\{n_3''\}\prec n_3'' \succ di\right]\{u_y\} + \prec \delta u_y \succ \left[\sum_{\alpha=1}^{n}\int_0^l (\frac{E_\alpha I_{yz\alpha}}{l^3})\{n_3''\}\prec n_3'' \succ di\right]\{u_z\}
\end{aligned} \tag{24}$$

3.4.1.2. The nonlinear part

The nonlinear part taken from eq. 17 is

$$\prec \delta u \succ [K_g]\{u\} = \tfrac{1}{2}\int_V f_x[\delta(u_y')^2 + \delta(u_z')^2]dV \tag{25}$$

when several elements participate in the nonlinear virtual work, the previous eq becomes

$$\prec \delta u \succ [K_g]\{u\} = \sum_{\alpha=1}^{n}\left[\int_0^l \frac{F_{x\alpha}}{2}[\delta(u'_y)^2 + \delta(u'_z)^2]dx\right] \tag{26}$$

in which α is the counter of the considered elements and is their total number.

$$\prec \delta u \succ [K_g]\{u\} = \prec \delta u_y \succ \left[\int_0^l \sum_{\alpha=1}^{n} \frac{F_{x\alpha}}{l}\{n_3'\}\prec n_3' \succ di\right]\{u_y\} + \prec \delta u_z \succ \left[\int_0^l \sum_{\alpha=1}^{n} \frac{F_{x\alpha}}{l}\{n_3'\}\prec n_3' \succ di\right]\{u_z\} \tag{27}$$

when n=2, as in the general case, then $\left[\int_0^l \sum_{\alpha=1}^{n} \frac{F_{x\alpha}}{l}\{n'_3\}\prec n'_3 \succ di\right]$ becomes $\left[\int_0^l \frac{(F_{x1}+F_{x2})}{l}\{n'_3\}\prec n'_3 \succ di\right]$. The linear and nonlinear stiffness matrices are obtained after performing the integrations in eqs 24 and 27 and are given in the appendix.

3.4.2. For bond-slip

The bond-slip expression given in eq.10 is substituted in the linear portion of the virtual work expression given in eq. 17 and the expression thus becomes

$$\prec \delta u \succ [K_b]\{u\} = \tfrac{1}{2}\int_v [E_b \delta(-u_{x1} + yu'_y + zu'_z + u_{x2})^2]dV = \prec \delta u \succ [\{^2 f\} - \{^1 f\}] \tag{28}$$

$$\begin{aligned}
\prec \delta u \succ [K_b]\{u\} &= \tfrac{1}{2}\int_0^l E_b A_b \left[\delta(u_{x1})^2 + \delta(u_{x2})^2 - 2\delta(u_{x1}u_{x2})\right]dx \\
&+ \tfrac{1}{2}\int_0^l E_b A_b y\left[-2\delta(u_{x1}u'_y) + 2\delta(u_{x2}u'_y)\right]dx \\
&+ \tfrac{1}{2}\int_0^l E_b A_b z\left[-2\delta(u_{x1}u'_z) + 2\delta(u_{x2}u'_z)\right]dx + \tfrac{1}{2}\int_0^l E_b A_b y^2\left[\delta\left(u'_y\right)^2\right]dx \\
&+ \tfrac{1}{2}\int_0^l E_b A_b z^2\left[\delta\left(u'_z\right)^2\right]dx + \tfrac{1}{2}\int_0^l E_b A_b yz\left[2\delta(u'_y u'_z)\right]dx
\end{aligned} \tag{29}$$

$$\begin{aligned}
&\prec \delta u \succ [K_b]\{u\} = \prec \delta u_{x1} \succ \left[\int_0^l lE_b A_b \{n_1\} \prec n_1 \succ di\right]\{u_{x1}\} + \prec \delta u_{x2} \succ \left[\int_0^l lE_b A_b \{n_1\} \prec n_1 \succ di\right]\{u_{x2}\} \\
&- \prec \delta u_{x2} \succ \left[\int_0^l lE_b A_b \{n_1\} \prec n_1 \succ di\right]\{u_{x1}\} - \prec \delta u_{x1} \succ \left[\int_0^l lE_b A_b \{n_1\} \prec n_1 \succ di\right]\{u_{x2}\} \\
&- \prec \delta u_{x1} \succ \left[\int_0^l E_b A_b y \{n_1\} \prec n'_3 \succ di\right]\{u_y\} - \prec \delta u_y \succ \left[\int_0^l E_b A_b y \{n'_3\} \prec n_1 \succ di\right]\{u_{x1}\} \\
&+ \prec \delta u_{x2} \succ \left[\int_0^l E_b A_b y \{n_1\} \prec n'_3 \succ di\right]\{u_y\} + \prec \delta u_y \succ \left[\int_0^l E_b A_b y \{n'_3\} \prec n_1 \succ di\right]\{u_{x2}\} \\
&- \prec \delta u_{x1} \succ \left[\int_0^l E_b A_b z \{n_1\} \prec n'_3 \succ di\right]\{u_z\} - \prec \delta u_z \succ \left[\int_0^l E_b A_b z \{n'_3\} \prec n_1 \succ di\right]\{u_{x1}\} \\
&+ \prec \delta u_{x2} \succ \left[\int_0^l E_b A_b z \{n_1\} \prec n'_3 \succ di\right]\{u_z\} + \prec \delta u_z \succ \left[\int_0^l E_b A_b z \{n'_3\} \prec n_1 \succ di\right]\{u_{x2}\} \\
&+ \prec \delta u_y \succ \left[\int_0^1 \frac{E_b y^2}{l}\{n'_3\} \prec n'_3 \succ di\right]\{u_y\} + \prec \delta u_z \succ \left[\int_0^1 (\frac{E_b z^2}{l})\{n'_3\} \prec n'_3 \succ di\right]\{u_z\} \\
&+ \prec \delta u_z \succ \left[\int_0^1 \frac{E_b zy}{l}\{n'_3\} \prec n'_3 \succ di\right]\{u_y\} + \prec \delta u_y \succ \left[\int_0^1 (\frac{E_b zy}{l})\{n'_3\} \prec n'_3 \succ di\right]\{u_z\}
\end{aligned} \tag{30}$$

where A_b is the area of the FRP per unit length of the segment.

The bond-slip matrix is obtained after performing the integrations in eq 30 and is given in the appendix.

Eqs.(24, 27 and 30) can be combined to give:

$$
\begin{aligned}
&\prec \delta u_{x1} \succ \left[\int_0^l \frac{E_1 A_1}{l}\{n_1'\} \prec n_1' \succ di\right]\{u_{x1}\} + \prec \delta u_{x1} \succ \left[\int_0^l (\frac{-E_1 S_{z1}}{l^2})\{n_1'\} \prec n_3'' \succ di\right]\{u_y\} \\
&+ \prec \delta u_{x1} \succ \left[\int_0^l (\frac{-E_1 S_{y1}}{l^2})\{n_1'\} \prec n_3'' \succ di\right]\{u_z\} \\
&+ \prec \delta u_{x1} \succ \left[\int_0^l l E_b A_b \{n_1\} \prec n_1 \succ di\right]\{u_{x1}\} - \prec \delta u_{x1} \succ \left[\int_0^l l E_b A_b \{n_1\} \prec n_1 \succ di\right]\{u_{x2}\} \\
&- \prec \delta u_{x1} \succ \left[\int_0^l E_b A_b z\{n_1\} \prec n_3' \succ di\right]\{u_z\} - \prec \delta u_{x1} \succ \left[\int_0^l E_b A_b y\{n_1\} \prec n_3' \succ di\right]\{u_y\} \\
&= \prec \delta u_{x1} \succ [\prec {}^2F_{x1A} \quad {}^2F_{x1B} \succ^T - \prec {}^1F_{x1A} \quad {}^1F_{x1B} \succ^T]
\end{aligned}
\tag{31a}
$$

$$
\begin{aligned}
&\prec \delta u_y \succ \left[\int_0^l (\frac{-E_1 S_{z1}}{l^2})\{n_3''\} \prec n_1' \succ di\right]\{u_{x1}\} + \prec \delta u_y \succ \left[\int_0^l (\frac{-E_2 S_{z2}}{l^2})\{n_3''\} \prec n_1' \succ di\right]\{u_{x2}\} \\
&+ \prec \delta u_y \succ \left[\sum_{\alpha=1}^n \int_0^l (\frac{E_\alpha I_{z\alpha}}{l^3})\{n_3''\} \prec n_3'' \succ di\right]\{u_y\} + \prec \delta u_y \succ \left[\sum_{\alpha=1}^n \int_0^l (\frac{E_\alpha I_{yz\alpha}}{l^3})\{n_3''\} \prec n_3'' \succ di\right]\{u_z\} \\
&+ \prec \delta u_y \succ \left[\int_0^l \sum_{\alpha=1}^n \frac{F_{x\alpha}}{l}\{n_3'\} \prec n_3' \succ di\right]\{u_y\} \\
&- \prec \delta u_y \succ \left[\int_0^l E_b A_b y\{n_3'\} \prec n_1 \succ di\right]\{u_{x1}\} + \prec \delta u_y \succ \left[\int_0^l E_b A_b y\{n_3'\} \prec n_1 \succ di\right]\{u_{x2}\} \\
&+ \prec \delta u_y \succ \left[\int_0^l \frac{E_b y^2}{l}\{n_3'\} \prec n_3' \succ di\right]\{u_y\} + \prec \delta u_y \succ \left[\int_0^l (\frac{E_b zy}{l})\{n_3'\} \prec n_3' \succ di\right]\{u_z\} \\
&= \prec \delta u_y \succ [\prec {}^2F_{yA} \quad \frac{{}^2M_{zA}}{l} \quad {}^2F_{yB} \quad \frac{{}^2M_{zB}}{l} \succ^T - \prec {}^1F_{yA} \quad \frac{{}^1M_{zA}}{l} \quad {}^1F_{yB} \quad \frac{{}^1M_{zB}}{l} \succ^T]
\end{aligned}
\tag{31b}
$$

$$
\begin{aligned}
&\prec \delta u_z \succ \left[\int_0^l (\frac{-E_1 S_{y1}}{l^2})\{n_3''\} \prec n_1' \succ di\right]\{u_{x1}\} + \prec \delta u_z \succ \left[\int_0^l (\frac{-E_2 S_{y2}}{l^2})\{n_3''\} \prec n_1' \succ di\right]\{u_{x2}\} \\
&+ \prec \delta u_z \succ \left[\sum_{\alpha=1}^n \int_0^l (\frac{E_\alpha I_{y\alpha}}{l^3})\{n_3''\} \prec n_3'' \succ di\right]\{u_z\} + \prec \delta u_z \succ \left[\sum_{\alpha=1}^n \int_0^l (\frac{E_\alpha I_{yz\alpha}}{l^3})\{n_3''\} \prec n_3'' \succ di\right]\{u_y\} \\
&+ \prec \delta u_z \succ \left[\int_0^l \sum_{\alpha=1}^n \frac{F_{x\alpha}}{l}\{n_3'\} \prec n_3' \succ di\right]\{u_z\} \\
&- \prec \delta u_z \succ \left[\int_0^l E_b A_b z\{n_3'\} \prec n_1 \succ di\right]\{u_{x1}\} + \prec \delta u_z \succ \left[\int_0^l E_b A_b z\{n_3'\} \prec n_1 \succ di\right]\{u_{x2}\} \\
&+ \prec \delta u_z \succ \left[\int_0^l \frac{E_b z^2}{l}\{n_3'\} \prec n_3' \succ di\right]\{u_z\} + \prec \delta u_z \succ \left[\int_0^l (\frac{E_b zy}{l})\{n_3'\} \prec n_3' \succ di\right]\{u_y\} \\
&= \prec \delta u_z \succ [\prec {}^2F_{zA} \quad \frac{{}^2-M_{yA}}{l} \quad {}^2F_{zB} \quad \frac{-{}^2M_{yB}}{l} \succ^T - \prec {}^1F_{zA} \quad \frac{-{}^1M_{yA}}{l} \quad {}^1F_{zB} \quad \frac{-{}^1M_{yB}}{l} \succ^T]
\end{aligned}
\tag{31c}
$$

$$
\begin{aligned}
&\prec \delta u_{x2} \succ \left[\int_0^l \frac{E_2 A_2}{l}\{n_1'\} \prec n_1' \succ di\right]\{u_{x2}\} + \prec \delta u_{x2} \succ \left[\int_0^l (\frac{-E_2 S_{z2}}{l^2})\{n_1'\} \prec n_3'' \succ di\right]\{u_y\} \\
&+ \prec \delta u_{x2} \succ \left[\int_0^l (\frac{-E_2 S_{y2}}{l^2})\{n_1'\} \prec n_3'' \succ di\right]\{u_z\} \\
&+ \prec \delta u_{x2} \succ \left[\int_0^l lE_b A_b \{n_1\} \prec n_1 \succ di\right]\{u_{x2}\} - \prec \delta u_{x2} \succ \left[\int_0^l E_b A_b y\{n_1\} \prec n_3' \succ di\right]\{u_y\} \\
&- \prec \delta u_{x2} \succ \left[\int_0^l E_b A_b z\{n_1\} \prec n_3' \succ di\right]\{u_z\} - \prec \delta u_{x2} \succ \left[\int_0^l lE_b A_b \{n_1\} \prec n_1 \succ di\right]\{u_{x1}\} \\
&= \prec \delta u_{x2} \succ [\prec {}^2F_{x2A} \quad {}^2F_{x2B} \succ^T - \prec {}^1F_{x2A} \quad {}^1F_{x2B} \succ^T]
\end{aligned}
\tag{31d}
$$

And upon simplification, the equilibrium equations (31a to 31d) are written in the form

$$[K_e]\{u\} + [K_g]\{u\} + [K_b]\{u\} = \{{}^2f\} - \{{}^1f\} \tag{32}$$

in which $[K_e]$, $[K_g]$ and $[K_b]$ are the linear, geometric and bond-slip stiffness matrices respectively, $\{u\}$ is the incremental displacement vector and $\{{}^1f\}$ and $\{{}^2f\}$ are the segment nodal forces at the beginning and the end of the incremental step.

The very simple form of the equilibrium equations is

$$[K_t]\{u\} = \{f\} \tag{33}$$

in which

$$[K_t] = [K_e] + [K_g] + [K_b] \tag{34}$$

The given procedure can be applied to problems with complete bond by combining elemental properties of the elements 1 and 2 and dropping out the bond-slip stiffness matrix. In this case each $[K]$ will be of order 10*10 instead of 12*12.

4. Stress-strain curves

The constitutive relations for concrete, steel, FRP and bond are schemetically shown in Fig.4.

4.1. Stress strain relationship for FRP

The stress-strain relationship for FRP is considered linear as shown in Fig.4.a

the incremental stress-strain relationship is given by

$$\delta f_f = G_f \delta \varepsilon_f \tag{35}$$

where G_f is the elemental FRP modulus of elasticity and is expressed as

$$G_f = \frac{f_{fu}}{\varepsilon_{fu}} = E_f \qquad \text{when} \qquad 0 \le \varepsilon_f \le \varepsilon_{fu} \tag{36}$$

in which f_f and ε_f are the FRP stress and strain respectively, f_{fu} and $\varepsilon_{f\ u}$ are the ultimate FRP stress and strain respectively and E_f is the modulus of elasticity of FRP.

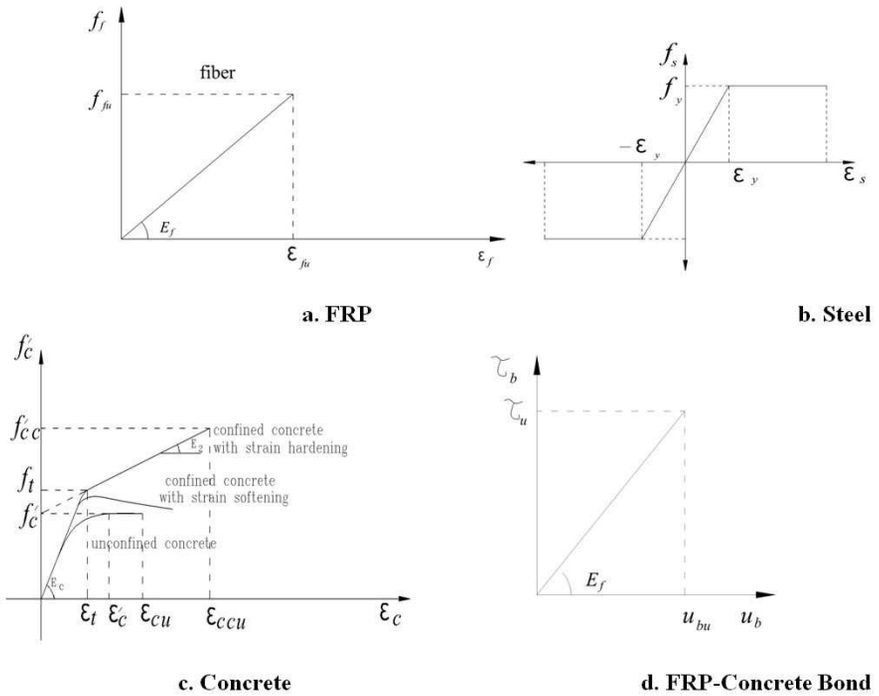

Figure 4. Stress-strain curves

4.2. Stress strain relationship for steel

For simplicity, the stress-strain relationship for the steel bars is considered to be an elastic-perfectly plastic curve neglecting steel hardening. The relationship is shown in Fig. 4.b.

The incremental stress-strain relationship is

$$\delta f_s = G_s \delta \varepsilon_s \tag{37}$$

where G_s is the incremental steel modulus of elasticity and is expressed as

http://dx.doi.org/10.5772/51446

$$G_s = \frac{f_y}{\varepsilon_y} = E_s \qquad \text{when} - \varepsilon_y \le \varepsilon_s \le \varepsilon_y \tag{38a}$$

$$G_s = 0 \qquad \text{when} \varepsilon_s \succ \varepsilon_y or \varepsilon_s \prec -\varepsilon_y \tag{38b}$$

in which f_s and ε_s are the steel stress and strain respectively, f_y and ε_y are the yield stress and yield strain respectively and E_s is the modulus of elasticity of steel.

4.3. Stress strain relationship for concrete

For unconfined concrete, the relationship adopted by Al-Noury and Chen [33] was chosen to express the first portion of the compressive stress-strain curve for concrete as a third-degree polynomial. The second portion is considered to be perfectly plastic as shown in Fig. 4.c. The incremental stress-strain relationships is expressed as:

$$\delta f_c = G_c \delta \varepsilon_c \tag{39}$$

where

$$G_c = \frac{f_c'}{\varepsilon_c'}\gamma_1 + 2\frac{f_c'}{\varepsilon_c'^2}(3 - 2\gamma_1)\varepsilon_c + 3\frac{f_c'}{\varepsilon_c'^3}(\gamma_1 - 2)\varepsilon_c^{\,2} \quad \text{when} \quad 0.0 \prec \varepsilon_c \le \varepsilon_c' \tag{40a}$$

$$G_c = 0.0 \qquad \text{when} \quad \varepsilon_c \succ \varepsilon_c' \tag{40b}$$

in which

$$\gamma_1 = \frac{E_c \varepsilon_c{}'}{f_c{}'} \quad , \quad \varepsilon_c' = 0.002 \quad \text{and} \quad E_c = 30000\sqrt{f_c'} \tag{41}$$

E_c= modulus of elasticity of concrete computed in t/m^2 while f_c' and ε_c' are the maximum unconfined concrete compressive strength and the corresponding strain respectively.

The stress-strain behavior of FRP-confined concrete is largely dependent on the level of FRP confinement. The bilinear stress-strain relationship suggested by Wu et al. [34] is shown in Fig. 4(c) and is adopted herein. The stress-strain curve of concrete confined with sufficient FRP displays a distinct bilinear curve with a second ascending branch as shown in Fig. 4(c). A minimum ratio of FRP confinement strength to unconfined concrete compressive strength f_l/f'_c of approximately 0.08 is provided to ensure an ascending second branch in the stress-strain curve. Confinement modulus (E_1) and confinement strength (f_l) are considered to be the two main factors affecting the performance of FRP-confined columns. The two factors are given as:

$$E_1 = \frac{1}{2}\rho_f E_f \tag{42a}$$

$$f_l = \frac{1}{2}\rho_f f_f \tag{42b}$$

where ρ_f is the volumetric ratio of FRP to concrete, which can be determined for a rectangular section as to a circular section with an equivalent diameter taken as the length of the diagonal of the rectangular section as follows:

$$\rho_f = \frac{4nt_f}{\sqrt{h^2 + b^2}} \tag{43}$$

where h and b are the bigger and smaller dimensions of the cross-section respectively, n is the number of FRP layers and t_f is the thickness of each layer.

The maximum FRP-confined concrete compressive strength and the ultimate axial strain of the FRP-confined concrete compressive stress-strain are given by Rocca et al. [35] as

$$f_{cc}' = f_c' + 3.3k_a f_l \tag{44a}$$

$$\varepsilon_{ccu} = \varepsilon_c'(1.5 + 12k_b \frac{f_l}{f_c'}(\frac{\varepsilon_{fe}}{\varepsilon_c'})^{0.45}) \leq 0.01 \tag{44b}$$

where k_a and k_b are efficiency factors that account for the geometry of the cross-section. In the case of rectangular columns, they depend on the effectively confined area ratio A_e/A_c and the side-aspect ratio h/b. These factors are given by the following expressions:

$$k_a = \frac{A_e}{A_c}\left(\frac{b}{h}\right)^2 \tag{45a}$$

$$k_b = \frac{A_e}{A_c}\left(\frac{b}{h}\right)^{0.5} \tag{45b}$$

$$\frac{A_e}{A_c} = \frac{1 - ((b/h)(h-2r)^2 + (h/b)(b-2r)^2)/(3A_g) - \rho_g{}^2}{1-\rho_g} \tag{46}$$

where A_g is the total cross-sectional area, ρ_g is the ratio of the longitudinal steel reinforcement to the cross-sectional area of a compression member and r is the corner radius of the cross-section.

The slope of the second branch E_2 is computed from the following equation considering the intercept of the second portion with the stress axis equal to f_c' for simplicity, Rocca et al. [35].

$$E_2 = \frac{f_{cc}' - f_c'}{\varepsilon_{ccu}} \tag{47}$$

The transition stress f_t and transition strain ε_t are given by the following equations

$$f_t = (1 + 0.0002E_1) f_c' \tag{48a}$$

$$\varepsilon_t = (1 + 0.0004E_1)\varepsilon_c' \tag{48b}$$

The maximum exerted confining pressure f_{lu} is attained when the circumferential strain in the FRP reaches its ultimate strain ε_{fu} corresponding to a tensile strength f_{fu} [36] and Eq. (42b) becomes

$$f_{lu} = \frac{1}{2}\rho_f f_{fu} = \frac{2 f_{fu} n t_f}{\sqrt{h^2 + b^2}} = \frac{2 n t_f E_f \varepsilon_{fe}}{\sqrt{h^2 + b^2}} \tag{49}$$

where $\sqrt{h^2 + b^2}$ is the equivalent diameter for non-circular cross-sections. The following equations express the elemental modulus of elasticity for confined concrete in terms of strain.

The effective strain ε_{fe} is computed as the product of an efficiency factor K_e and the ultimate FRP tensile strain ε_{fu}. The factor K_e is to account for the difference between the actual rupture strain observed in FRP-confined concrete specimens and the FRP material rupture strain determined from tensile coupon testing, Wu et al. [34]. The factor ranges from 0.55 to 0.61 and is taken 0.586 in this study.

$$G_c = E_c \quad \text{when} \quad 0 \le \varepsilon_c \le \varepsilon_t \tag{50a}$$

$$G_c = E_2 \quad \text{when} \quad \varepsilon_t \prec \varepsilon_c \le \varepsilon_{ccu} \tag{50b}$$

4.4. Stress strain relationship for FRP-Concrete Bond

The relationship is shown in Fig. 4.d.

The incremental stress-strain relationship is

$$\delta\tau_b = G_b \delta u_b \tag{51}$$

where G_b is the incremental steel modulus of elasticity and is expressed as

$$G_b = \frac{\tau_b}{u_b} = E_b \quad \text{when} \quad 0 \le u_b \le u_{bu} \tag{52}$$

in which τ_b and u_b are the steel stress and strain respectively, τ_b and u_b are the yield stress and yield strain respectively and E_b is the bond elastic stiffness.

5. Steps of solution followed by the developed program

The mixed procedure is utilized to solve the nonlinear problem. This procedure utilizes a combination of the incremental and iterative (Newton-Raphson) schemes. The load is applied incrementally and after each increment successive iterations are performed. Steps of the solution are then introduced.

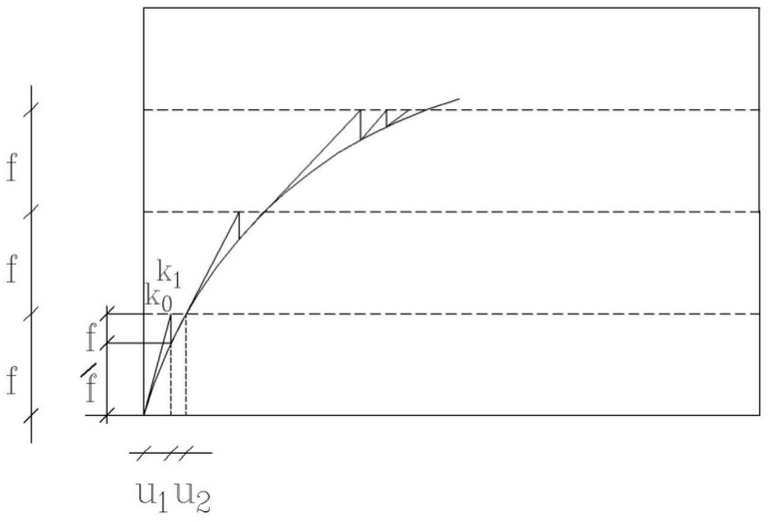

Figure 5. Incremental-iterative method

The mixed procedure is utilized herein to solve the nonlinear problem. This procedure utilizes a combination of the incremental and iterative (Newton-Raphson) schemes. The load is applied incrementally and after each increment successive iterations are performed. The method is illustrated in fig.5.

The combined method is summarized in the following steps:

1. Apply the first increment of load {f} and compute $[K_o]$ assuming no cracks and full bond between the concrete element and the FRP element at the beginning. Compute the displacements $\{u_1\}$ by solving the equation $[K_o]\{u_1\}=\{f\}$

http://dx.doi.org/10.5772/51446

2. Compute [K_1] based on the displacement {u_1} then compute the load {f} from the equation $\{f'\}=[K_1]\{u_1\}$

3. Compute {Δf} as the difference between the applied load {f} and the deduced load $\{f'\}$. Then compute the corresponding displacements {u_2} by solving the equation $[K_1]\{u_2\}=\{\Delta f\}$

4. Repeat steps 2 and 3 until {Δf} becomes very small.

5. Repeat all steps again for the next increment.

6. Numerical examples

Two examples are given below. The first example considers a rectangular column fully confined with FRP. Complete bond is considered. The second example is a beam strengthened with FRP on the tension side. In this example the slip between the two elements is considered.

Example 1: The verification of the method is plotted in Fig.6 against experimental results given by Chaallal and Shahawy [1]. The column has across-section of 0.35*0.2 m^2 and length 2.1m. The concrete has a compression strength 25 MPa and the column is reinforced with 4 grade 60 steel bars of diameter 19 mm each. The steel bars are of 406 MPa yield stress and 206 GPa modulus of elasticity. The specimens are confined with 1mm of carbon fiber reinforced polymer of tensile strength 530 MPa and tensile modulus of elasticity 44 GPa. This gives a confinement ratio, f_l/f_c'=0.103. The present procedure of analysis was adopted to the same specimens and interaction diagrams were plotted. The present results show great accordance with the previous work.

A slight difference in results is observed. It is owed to the provision of corbels in the specimens of Chaallal and Shahawy. They provided large corbels at the ends of the specimens to receive a single load source applied eccentrically thus simulating the combined stress effects in columns. The corbels increased the overall stiffness of the beam column and thus the capacity of loads.

It should be noted that all wraps were characterized by a bidirectional oriented fibers ($0^0/90^0$) applied along the entire height of the columns. As recommended by ACI 440.2R-02 [37]. The enhancement is only of the significance in members where compression failure is the controlling mode Nanni [38]. This strength enhancement is due to the confining effect of the FRP. When the column is subjected to axial load F_x and moment M_z such that their coordinates lie below the balanced point, the column is considered to be unconfined. This is owed to the limited value of F_x which is considered insufficient to dilate the concrete in the hoop direction thus failing to activate the FRP wrapping effect to confine the concrete. In the present analysis where the wraps are of bidirectional fibers, the point of pure bending is computed accounting for the FRP in the longitudinal direction and its contribution to the

flexural capacity according to ACI440.2R-02 [37]. This case was also set by Chaallal and Shahawy [1]. Fig.7shows the plots of the column subjected to uniaxial bending Mz and My.

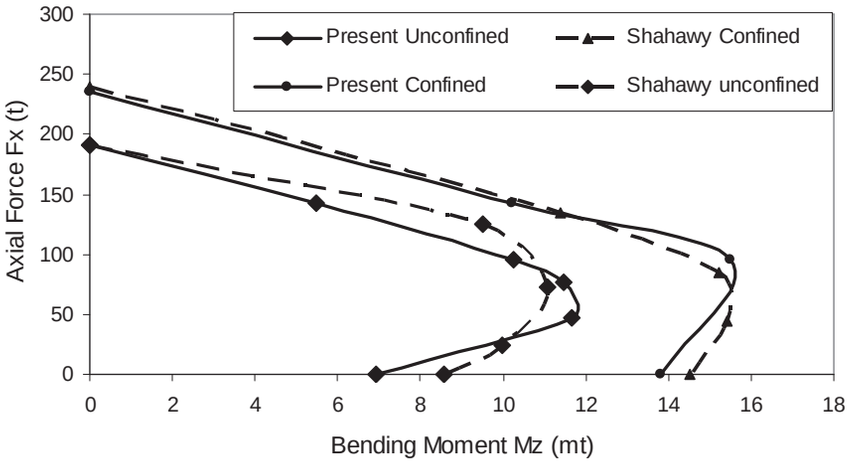

Figure 6. Verification against Shahawy

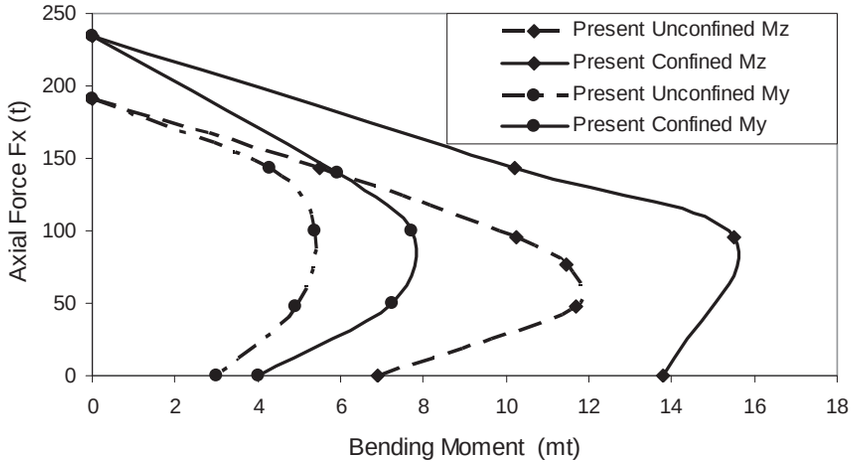

Figure 7. Uniaxial Moments About z and y axes

As expected, the capacity of the about the about the y-axis is less than that about the z-axis. The same model was also subjected to biaxial bending at two axial load levels, namely: Fx=0 and Fx=0.7. The plots of the contour lines of the confined and unconfined columns are given in Figs.(8 and 9).

http://dx.doi.org/10.5772/51446

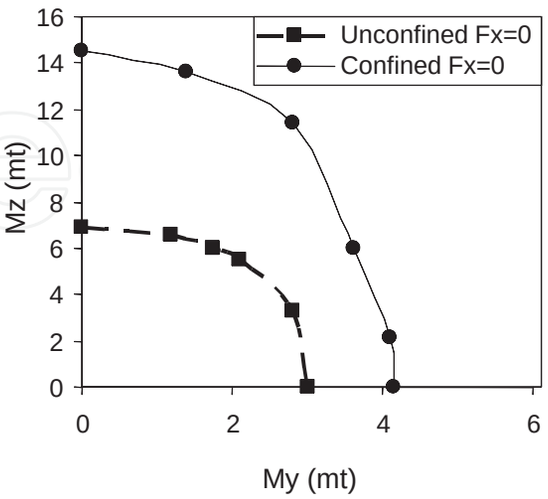

Figure 8. Contour lines (Fx=0.0)

Example 2:The problem of bond-slip was verified against Aprile et al.[39]. A simply supported rectangular beam of length 2.9m loaded by two forces, each=F at the middle third of the beam. The cross-section is 0.3*0.2 m^2. Top reinforcement is 226 mm^2, bottom reinforcement is 339 mm^2. the beam is strengthened at the bottom by carbon FRP of width 50 mm and 1.2 mm thickness. The concrete has a compression strength 25 MPa. The steel bars are of 460 MPa yield strength and 210 GPa modulus of elasticity. The carbon fiber reinforced polymer is of tensile strength 2400 MPa and tensile modulus of elasticity 150 GPa. The epoxy resin is of 100 MPa compressive strength and 12.8 GPa modulus of elasticity. The concrete element is considered supported on a roller at one end and hinged at the other end. While the FRP element is considered to be supported on rollers at both ends. Fig.10 shows the verification of the present analysis if the beam considering bond-slip against Aprile. The curves are plots of the midspan deflection of the beam against the applied force (2F). A slight difference is observed between the two curves. Also, a plot of the reference beam, with no FRP was plotted as reference beam. Another plot of the beam with full bond between the concrete and the FRP was plotted. At the maximum deflection of the beam with bond-slip, the reference beam shows nearly 15% decrease in the load capacity while the beam with complete bond achieves nearly 20% increase in the load capacity. In addition, the later beam undergoes greater deflection and the highest capacity. The curves show two points of remarkable change in slope indicating remarkable loss of strength in the beam. The lower point indicates concrete cracking in the middle third of the beam, at the location of the applied concentrated load. The upper point indicates the start of yield of the bottom steel reinforcement.

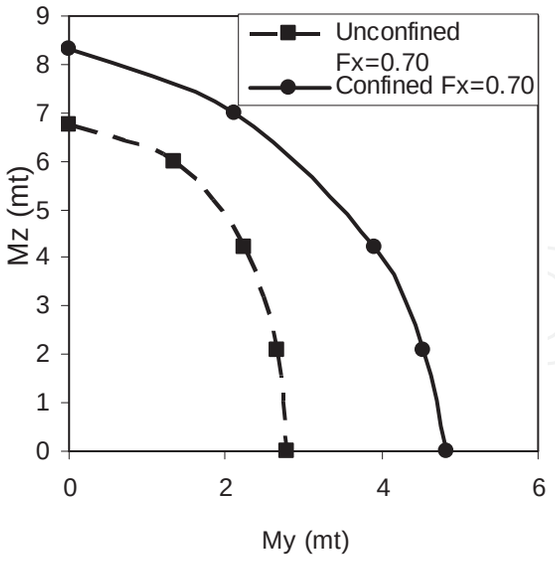

Figure 9. Contour lines (Fx=0.70)

7. Summary and conclusions

The FEA together with the FMM were utilized to solve the problem of RC strengthened with FRP. The structural member solved can be of any slenderness ratio, under any loading and can have any end conditions. The FRP wraps can be totally or partially bonded to the concrete member. The elastic, geometric and bond-slip stiffness matrices of the member in the three-dimension were deduced and given in an appendix.

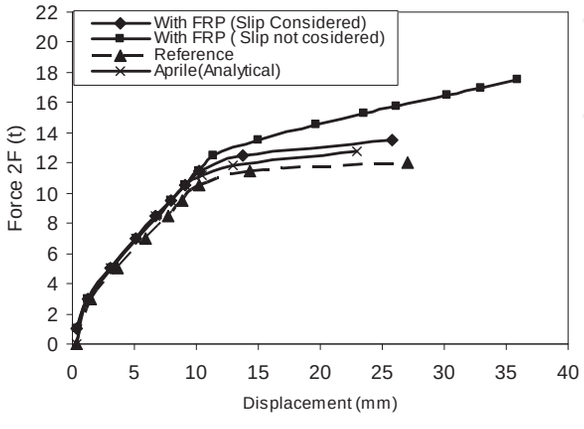

Figure 10. Force-Deflection Diagrams

http://dx.doi.org/10.5772/51446

	u_{x1}	u_y	u_z	θ_y	θ_z	u_{x2}	u_{x1}	u_y	u_z	θ_y	θ_z	u_{x2}
F_{x1}	$\frac{E_1A_1}{l}$			$\frac{E_1S_{y1}}{l}$	$\frac{-E_1S_{z1}}{l}$		$\frac{-E_1A_1}{l}$			$\frac{-E_1S_{y1}}{l}$	$\frac{E_1S_{z1}}{l}$	
F_y		$\frac{12\sum_{\alpha=1}^{n}(E_\alpha I_{z\alpha})}{l^3}$	$\frac{12\sum_{\alpha=1}^{n}(E_\alpha I_{yz\alpha})}{l^3}$	$\frac{-6\sum_{\alpha=1}^{n}(E_\alpha I_{yz\alpha})}{l^2}$	$\frac{6\sum_{\alpha=1}^{n}(E_\alpha I_{z\alpha})}{l^2}$			$\frac{-12\sum_{\alpha=1}^{n}(E_\alpha I_{z\alpha})}{l^3}$	$\frac{-12\sum_{\alpha=1}^{n}(E_\alpha I_{yz\alpha})}{l^3}$	$\frac{-6\sum_{\alpha=1}^{n}(E_\alpha I_{yz\alpha})}{l^2}$	$\frac{6\sum_{\alpha=1}^{n}(E_\alpha I_{z\alpha})}{l^2}$	
F_z			$\frac{12\sum_{\alpha=1}^{n}(E_\alpha I_{y\alpha})}{l^3}$	$\frac{-6\sum_{\alpha=1}^{n}(E_\alpha I_{y\alpha})}{l^2}$	$\frac{6\sum_{\alpha=1}^{n}(E_\alpha I_{yz\alpha})}{l^2}$			$\frac{-12\sum_{\alpha=1}^{n}(E_\alpha I_{yz\alpha})}{l^3}$	$\frac{-12\sum_{\alpha=1}^{n}(E_\alpha I_{y\alpha})}{l^3}$	$\frac{-6\sum_{\alpha=1}^{n}(E_\alpha I_{y\alpha})}{l^2}$	$\frac{6\sum_{\alpha=1}^{n}(E_\alpha I_{zy\alpha})}{l^2}$	
M_y				$\frac{4\sum_{\alpha=1}^{n}(E_\alpha I_{y\alpha})}{l}$	$\frac{-4\sum_{\alpha=1}^{n}(E_\alpha I_{yz\alpha})}{l}$	$\frac{E_2S_{y2}}{l}$	$\frac{-E_1S_{y1}}{l}$	$\frac{6\sum_{\alpha=1}^{n}(E_\alpha I_{yz\alpha})}{l^2}$	$\frac{6\sum_{\alpha=1}^{n}(E_\alpha I_{y\alpha})}{l^2}$	$\frac{2\sum_{\alpha=1}^{n}(E_\alpha I_{y\alpha})}{l}$	$\frac{-2\sum_{\alpha=1}^{n}(E_\alpha I_{zy\alpha})}{l}$	$\frac{-E_2S_{y2}}{l}$
M_z					$\frac{4\sum_{\alpha=1}^{n}(E_\alpha I_{z\alpha})}{l}$	$\frac{-E_2S_{z2}}{l}$	$\frac{E_1S_{z1}}{l}$	$\frac{-6\sum_{\alpha=1}^{n}(E_\alpha I_{z\alpha})}{l^2}$	$\frac{-6\sum_{\alpha=1}^{n}(E_\alpha I_{yz\alpha})}{l^2}$	$\frac{-2\sum_{\alpha=1}^{n}(E_\alpha I_{yz\alpha})}{l}$	$\frac{2\sum_{\alpha=1}^{n}(E_\alpha I_{z\alpha})}{l}$	$\frac{E_2S_{z2}}{l}$
F_{x2}						$\frac{E_2A_2}{l}$				$\frac{-E_2S_{y2}}{l}$	$\frac{E_2S_{z2}}{l}$	$\frac{-E_2A_2}{l}$
F_{x1}							$\frac{E_1A_1}{l}$			$\frac{E_1S_{y1}}{l}$	$\frac{-E_1S_{z1}}{l}$	
F_y								$\frac{12\sum_{\alpha=1}^{n}(E_\alpha I_{z\alpha})}{l^3}$	$\frac{12\sum_{\alpha=1}^{n}(E_\alpha I_{yz\alpha})}{l^3}$	$\frac{6\sum_{\alpha=1}^{n}(E_\alpha I_{yz\alpha})}{l^2}$	$\frac{-6\sum_{\alpha=1}^{n}(E_\alpha I_{z\alpha})}{l^2}$	
F_z									$\frac{12\sum_{\alpha=1}^{n}(E_\alpha I_{y\alpha})}{l^3}$	$\frac{6\sum_{\alpha=1}^{n}(E_\alpha I_{y\alpha})}{l^2}$	$\frac{-6\sum_{\alpha=1}^{n}(E_\alpha I_{yz\alpha})}{l^2}$	
M_y										$\frac{4\sum_{\alpha=1}^{n}(E_\alpha I_{y\alpha})}{l}$	$\frac{-4\sum_{\alpha=1}^{n}(E_\alpha I_{yz\alpha})}{l}$	$\frac{E_2S_{y2}}{l}$
M_z											$\frac{4\sum_{\alpha=1}^{n}(E_\alpha I_{z\alpha})}{l}$	$\frac{-E_2S_{z2}}{l}$
F_{x2}												$\frac{E_2A_2}{l}$

Appendix 1. Linear Stiffness Matrix [K_e]

	u_{x1}	u_y	u_z	θ_y	θ_z	u_{x2}	u_{x1}	u_y	u_z	θ_y	θ_z	u_{x2}
F_{x1}												
F_y		$\frac{6}{5l}$			$\frac{1}{10}$			$\frac{-6}{5l}$			$\frac{1}{10}$	
F_z			$\frac{6}{5l}$	$\frac{-1}{10}$					$\frac{-6}{5l}$	$\frac{-1}{10}$		
M_y				$\frac{2l}{15}$					$\frac{1}{10}$	$\frac{-l}{30}$		
M_z					$\frac{2l}{15}$			$\frac{-1}{10}$			$\frac{-l}{30}$	
F_{x2}												
F_{x1}												
F_y								$\frac{6}{5l}$			$\frac{-1}{10}$	
F_z									$\frac{6}{5l}$	$\frac{1}{10}$		
M_y										$\frac{2l}{15}$		
M_z											$\frac{2l}{15}$	
F_{x2}												

All the elements of the geometric stiffness matrix are multiplied by the factor $\sum_{\alpha=1}^{n} F_{x\alpha}$ which in the general case when α=2, the previous term is ($F_{x1} + F_{x2}$).

Appendix 2. Nonlinear Stiffness Matrix [K_g].

	u_{x1}	u_y	u_z	θ_y	θ_z	u_{x2}	u_{x1}	u_y	u_z	θ_y	θ_z	u_{x2}
F_{x1}	$\frac{lE_bA_b}{3}$	$\frac{E_bA_by}{2}$	$\frac{E_bA_bz}{2}$	$\frac{lE_bA_bz}{12}$	$\frac{-lE_bA_by}{12}$	$\frac{-lE_bA_b}{3}$	$\frac{lE_bA_b}{6}$	$\frac{-E_bA_by}{2}$	$\frac{-E_bA_bz}{2}$	$\frac{-lE_bA_bz}{12}$	$\frac{lE_bA_by}{12}$	$\frac{-lE_bA_b}{6}$
F_y		$\frac{6E_bA_by^2}{5l}$	$\frac{6E_bA_byz}{5l}$	$\frac{-E_bA_byz}{10}$	$\frac{E_bA_by^2}{10}$	$\frac{-E_bA_by}{2}$	$\frac{E_bA_by}{2}$	$\frac{-6E_bA_by^2}{5l}$	$\frac{-6E_bA_byz}{5l}$	$\frac{-E_bA_byz}{10}$	$\frac{E_bA_by^2}{10}$	$\frac{-E_bA_by}{2}$
F_z			$\frac{6E_bA_bz^2}{5l}$	$\frac{-E_bA_bz^2}{10}$	$\frac{E_bA_byz}{10}$	$\frac{-E_bA_bz}{2}$	$\frac{E_bA_bz}{2}$	$\frac{-6E_bA_byz}{5l}$	$\frac{-6E_bA_bz^2}{5l}$	$\frac{-E_bA_bz^2}{10}$	$\frac{E_bA_byz}{10}$	$\frac{-E_bA_bz}{2}$
M_y				$\frac{2lE_bA_bz^2}{15}$	$\frac{-2lE_bA_byz}{15}$	$\frac{-lE_bA_bz}{12}$	$\frac{-lE_bA_bz}{12}$	$\frac{E_bA_byz}{10}$	$\frac{E_bA_bz^2}{10}$	$\frac{-lE_bA_bz^2}{30}$	$\frac{lE_bA_bzy}{30}$	$\frac{lE_bA_bz}{12}$
M_z					$\frac{2lE_bA_by^2}{15}$	$\frac{lE_bA_by}{12}$	$\frac{lE_bA_by}{12}$	$\frac{-E_bA_by^2}{10}$	$\frac{-E_bA_byz}{10}$	$\frac{lE_bA_bzy}{30}$	$\frac{-lE_bA_by^2}{30}$	$\frac{-lE_bA_by}{12}$
F_{x2}						$\frac{lE_bA_b}{3}$	$\frac{-lE_bA_b}{6}$	$\frac{E_bA_by}{2}$	$\frac{E_bA_bz}{2}$	$\frac{lE_bA_bz}{12}$	$\frac{-lE_bA_by}{12}$	$\frac{lE_bA_b}{6}$
F_{x1}							$\frac{lE_bA_b}{3}$	$\frac{-E_bA_by}{2}$	$\frac{-E_bA_bz}{2}$	$\frac{lE_bA_bz}{12}$	$\frac{-lE_bA_by}{12}$	$\frac{-lE_bA_b}{3}$
F_y			Symmetric					$\frac{6E_bA_by^2}{5l}$	$\frac{6E_bA_byz}{5l}$	$\frac{E_bA_byz}{10}$	$\frac{-E_bA_by^2}{10}$	$\frac{E_bA_by}{2}$
F_z									$\frac{6E_bA_bz^2}{5l}$	$\frac{E_bA_bz^2}{10}$	$\frac{-E_bA_byz}{10}$	$\frac{E_bA_bz}{2}$
M_y										$\frac{2lE_bA_bz^2}{15}$	$\frac{-2lE_bA_byz}{15}$	$\frac{-lE_bA_bz}{12}$
M_z											$\frac{2lE_bA_by^2}{15}$	$\frac{lE_bA_by}{12}$
F_{x2}												$\frac{lE_bA_b}{3}$

Appendix 3. Bond-slip Stiffness Matrix [K_b]

Two examples were studied. The first example considers a rectangular column fully confined with FRP. Complete bond was considered. Contour lines can be plotted at any load level. The second example is a beam strengthened with FRP on the tension side. In this example the slip between the two elements was considered. Load-deflection diagrams show that there exist two points of drop in stiffness, the first is due to concrete cracking under the concentrated loads and the second is due to the yield of steel. Extensive research is required to study the effect of the aspect ratio of the concrete cross-section, the strength of the concrete, the strength of FRP, the thickness of FRP and the properties of the epoxy resin used.

Author details

Manal K. Zaki*

Address all correspondence to: manalzaki64@yahoo.com.

Department of Civil and Construction Engineering, Higher Technological Institute, 6th October Branch, Guiza Egypt

References

[1] Challal, O., Shahawy, M., & Hassan, M. (2003). Performance of axially loaded short rectangular columns strengthened with carbon fiber-reinforced polymer wrapping. *J Comp Const, ASCE*, 7(3), 200-208.

[2] Tastani, S. P., & Pantazopoulou, S. J. (2008). Detailing procedures for seismic rehabiliation of reinforced concrete members wiyh fiber reinforced polymers. *Engineering Structures*, 2, 450-461.

[3] Ozcan, O., Binici, B., & Ozceke, G. (2008). Improving seismic performance of dificient reinforced concrete columns using carbon fiber reinfored polymers. *Engineering Structures*, 30(6), 1632-1646.

[4] Ozcan, O., Binici, B., & Ozceke, G. (2010). Seismic strengthening of rectangular reinforced concrete columns using fiber reinfored polymers. *Engineering Structures*, 32(4), 964-973.

[5] Kachlakev, D., Thomas, M., & Yim, S. (2001). Finite element modeling of reinforced concrete structures strengthened with frp laminates. *Report for Oregon Department of Ransportation Salem*.

[6] Li, G. K., Su-Seng, P. S., Helms, J. E., & Stukklefield, M. A. (2003). Investigation into frp repaired RC columns. *J Comp. Struct*, 62, 83-80.

[7] Yan, Z., Pantelides, C. P., & Reaveley, L. D. (2006). Fiber reinforced polymer jacketed and shape-modified compression members: I-experimental behavior. *Struct J, ACI*, 103(6), 885-893.

[8] Purushotham, B. R., Alagusundaramoorthy, P., & Sundaravalivelu, R. (2009). Retrofitting of RC piles using GFRP composites. *Journal of Civil Engineering, KSCE*, 13(1), 39-47.

[9] Kaba, S. A., & Mahin, S. A. (1984). Refined modeling of reinforced concrete columns for seismic analysis. *Report No. UBC/EERC-84/3. Ca: University of California, Berkeley*.

[10] Bresler, B. Design criteria for reinforced columns under axial load and biaxial bending. ACI J. (1960). , 32(5), 481-490.

[11] Bernardo, A. L. (2007). Investigation of biaxial bending of reinforced concrete columns through fiber method modeling. *Journal of Research in Science, Computing and Engineering*, 4(3), 61-73.

[12] Newmark, M. N., Siess, C. P., & Viest, I. M. (1951). Tests and analysis of composite beams with incomplete interaction. *Proceedings of the Society for Experimental Stress Analysis*, 9, 175-92.

[13] Arizumi, Y., Hamada, S., & Kajita, T. (1981). Elastic-plastic analysis of composite beams with incomplete interaction by finite element method. *Comp. Struct.*

[14] Daniel, B. J., & Crisinel, M. (1993). Composite slab behavior and strength analysis. *Part I: Calculation procedure. J. Struct. Engrg.*, ASCE, 119(1), 16-35.

[15] Salari, M. R., Spacone, E., Shing, P. B., & Frangopol, D. M. (1997). Behavior of composite structures under cyclic loading. Build. *To Last, Proc., ASCE Struct.Congr. VX, Kempner Jr. L and Brown CB, eds.*, ASCE, New York, 1.

[16] Gara, F., Ranzi, G., & Leoni, G. (2006). Displacement-based formulations for composite beams with longitudinal slip and vertical uplift. *Internat J Numer Methods Engrg.*, 65(8), 1197-220.

[17] Ranzi, G., Gara, F., & Ansourian, P. (2006). General method of analysis for composite beams with longitudinal and transverse partial interaction. *Computers and Structures*.

[18] Salari, M. R., & Spacone, E. (2001). Finite element formulations of one-dimensional elements with bond-slip. *Eng Struct.*, 23, 815-26.

[19] Valipour, Goudarzi. H., & Bradford, M. M.A.(2012). A new shape function for tapered three-dimensional beams with flexible connections. Journal Of Constructional Steel Research , 70, 43-50.

[20] Dall'Asta, A., & Zona, A. (2004). Three-field mixed formulation for the nonlinear analysis of composite beams with deformable shear connection. *Finite Elem Anal Design*, 40, 425-48.

[21] Ayoub, A., & Filippou, F. C. (2002). Mixed formulation of nonlinear steel-concrete composite beam element. *J Struct Eng*, 126(3), 371-81.

[22] Grihammar, U. A., & Gopu, V. K. A. Composite beam-columns with interlayer slip-Exact analysis. J Struct Eng. ASCE (1993).

[23] Grihammar, U.A.P. (2007). Exact static analysis of partially composite beams and beam-columns. *Int J mech Sci*, 49, 139-55.

[24] Čas, B., Sage, M., & Planinc, I. (2004). Non-linear finite element analysis of composite planar frames with interlayer slip. *Comput Struct.*, 82, 1901-12.

[25] Pi, Y. L., Bradford, M. A., & Uy, B. (2006). second order nonlinear inelastic analysis of composite steel-concrete members. I: Theory. *J Struct Eng.*, ASCE, 132(5), 751-61.

[26] Krawczyk, P., Frey, F., & Zielinsky, A. P. (2007). Large deflections of laminated beams with interlayer slips Part 1: Model development. *Eng comput.*, 24(1), 17-32.

[27] Krawczyk, P., & Rebora, B. (2007). Large deflections of laminated beams with interlayer slips Part 2: finite element development. *Eng comput.*, 24(1), 33-51.

[28] Battini, J. M., Nguyen, Q. H., & Hjiaj, M. (2009). Non-linear finite element analysis of composite beams with interlayer slip. *Comput Struct.*, 87, 904-12.

[29] Nguyen, Q. H., & Hjiaj, M. (2011). Exact finite element model for shear-deformable two-layer beams with discrete shear connection. *Finite Elements in Analysis and Design*, 47, 718-727.

[30] Sousa Jr., J. B. M., Oliveira, C. E. M., & da Silva, A. R. (2010). Displacement-based non-linear finite element analysis of composite beams with partial interaction. *Journal of constructional Steel Research.*, 66, 772-779.

[31] Zaki, M.K. (2011). Investigation of FRP strengthened circular columns under biaxial bending. *Engineering Structures*, 33(5), 1666-1679.

[32] Yang, Y. B., & Mc Graw, W. (1986). Stiffness Matrix for Geometric Nonlinear Analysis. *Journal of Structural Engineering*, ASCE, 112, 853-877.

[33] Al-Noury, S. I., & Chen, W. F. (1982). Behavior and design of reinforced and composite concrete sections. *Journal of Structural Division*, ASCE, 17169, 1266-1284.

[34] Wu, G., Lu, Z. T., & Wu, Z. S. (2006). Strength and ductility of concrete cylinders confined with FRP composites. *Construction and Building Materials*, 20, 134-148.

[35] Rocca, S., Galati, N., & Nanni, A. (2009). Interaction diagram methodology for desgin of FRP-confined reinforced concrete columns. *Construction and Building Materials*, 23, 1508-1520.

[36] Wu, G., Lu, Z. T., & Wu, Z. S. (2003). Stress-strain relationship for FRP-confined concrete cylinders. *Proceedings of the 6th international symposium on FRP reinforcement for concrete structures (FRPRCS), Singapor*, 552-560.

[37] American Concrete Institute. (2002). ACI440.2R, Guide for the design and construction of externally bonded FRP systems for strengthening of concrete structures. *Farmington Hills, MI, USA: American Concrete Institute*.

[38] Nanni, A., & Bradford, N.M. (1995). FRP jacketed concrete under uniaxial compression. *Constr. and Build. Mat.*, 9(2), 115-124.

[39] Aprile, A., Spacone, E., & Limkatanyu, S. (2001). Role of bond in RC beams strengthened with steel and FRP plates. *Journal of Structural Division*, ASCE, 22694, 1445-11452.

IntechOpen